Supporting information

Surface Modification of $Na_2Ti_3O_7$ Nanofibre Arrays by N-doped Graphene Quantum Dots as Advanced Anodes for Sodium-ion Batteries with Ultra-stable and High-rate Capability

Dezhi Kong [†], Ye Wang [†,‡], Shaozhuan Huang [†], Yew Von Lim [†], Jun Zhang [§], Linfeng Sun [†], Bo Liu [†], Tupei Chen [§], Pablo Valdivia y Alvarado[†], and Hui Ying Yang [†,*]

[†] *Pillar of Engineering Product Development, Singapore University of Technology and Design, 8 Somapah Road, Singapore 487372, Singapore.*

[‡] *Key Laboratory of Material Physics of Ministry of Education, School of Physics and Engineering, Zhengzhou University, Zhengzhou 450052, China*

[§] *School of Electrical and Electronic Engineering, Nanyang Technological University, Singapore 639798, Singapore.*

** Corresponding author. E-mail address: yanghuiying@sutd.edu.sg (H.Y. Yang).*

Supplementary method:

Preparation of N-doped carbon-wrapped $Na_3V_2(PO_4)_3$ (mark as $Na_3V_2(PO_4)_3$@NC) cathode material

For the synthesis of $Na_3V_2(PO_4)_3$@NC, 0.546 g vanadium trioxide (3 mmol, V_2O_3), 1.08 g sodium dihydrogen phosphate (9 mmol, NaH_2PO_4) and 0.96 g citric acid (5 mmol, $C_6H_8O_7$) were dissolved in distilled water with continuous stirring for 1 h to form a uniform and dark blue sol. Citric acid was used here not only as a carbon source but also as a chelating agent. Subsequently, the dark blue sol mixture was heated to 120 °C until all the solvent evaporated. Finally, $Na_3V_2(PO_4)_3$@NC power was obtained by annealing the dried gel precursor at 350 °C for 3 h and then at 800°C for 8 h with the heating rate of 5 °C/min, under Ar atmosphere.

The reference $Na_3V_2(PO_4)_3$@NC/CTs electrode was prepared by mixing the $Na_3V_2(PO_4)_3$@NC power, acetylene black, and poly(vinyl difluoride) in N-methyl pyrrolidone at 80:10:10 mass ratio and then casting the slurry on carbon textiles. Afterward, the electrode was dried under vacuum at 120 °C for 6 h.

The capacity balance of cathode and anode in full SIB

The theoretical reversible capacity of anode ($Na_2Ti_3O_7$) and cathode ($Na_3V_2(PO_4)_3$) is about 177 and 120 mAh g^{-1}, respectively.[1-3] The capacity of anode is excess 10 % to prevent the precipitation of Na. Thus, the mass ratio of anode and cathode is carefully calculated as 1 : 1.34 as follows:

$$m_{cathode}/m_{anode} = C_{anode}/(1+10\ \%)C_{cathode} = 177/(1+10\ \%)/120 = 1.34 \qquad (1)$$

Calculation details for the separation of the diffusion-controlled and capacitive-controlled charge contributions

The total current (or charge) of the electrode at a certain potential can be divided into two parts, described as [4,5]:

$$i(V) = k_1 v + k_2 v^{1/2} \qquad (2)$$

or

$$i(V)/v^{1/2} = k_1 v^{1/2} + k_2 \qquad (3)$$

on the base of the power law relationship of $i = k_1 v$ for non-diffusion limited

(capacitive-controlled) processes and $i = k_2 v^{1/2}$ for solid-state diffusion-controlled processes. The current values at a certain potential can be determined by the cyclic voltammograms at various scan rates of 0.1-5.0 mV s^{-1}. By plotting curves of $i(V)/v^{1/2}$ vs. $v^{1/2}$ (v vs. from 0.1 to 5.0 mV s^{-1}), the values of k_1 (slop) and k_2 (intercept) at a certain potential can be determined according to formula (3). When the series k_1 and k_2 values at different potentials are quantified, the values of $k_1 v$ and $k_2 v^{1/2}$ at a fixed scan rate (v) can be determined, thus the capacitive-controlled ($k_1 v$) and diffusion-controlled ($k_2 v^{1/2}$) currents are separated.

Calculation of energy density and power density

Based on the total mass of the active materials from the positive and negative electrodes, the energy density (E, Wh/kg) and power density (P, W/kg) were calculated based on the following formula [6,7]:

$$E = \frac{\int_{t_1}^{t_2} V(t) \cdot I(t) \cdot \mathrm{d}t}{m} = \Delta V \times \frac{I}{m} \times \Delta t \quad (4)$$

$$P = \frac{E}{\Delta t} = \Delta V \times \frac{I}{m} \quad (5)$$

$$\Delta V = \frac{V_{\max} + V_{\min}}{2} \quad (6)$$

where V is the cell potential (V), $V_{\min}$ and $V_{\max}$ are the potential at the initial and final charge curves during galvanostatic measurements, respectively; I is the current density (A kg^{-1}); t is the time (h), t_1 is the time at which the cell is fully discharged, t_2 is the time at which the cell is fully charged, and Δt is the discharge time (h); m is the total mass of the active material in both the electrodes.

Supplementary figures:

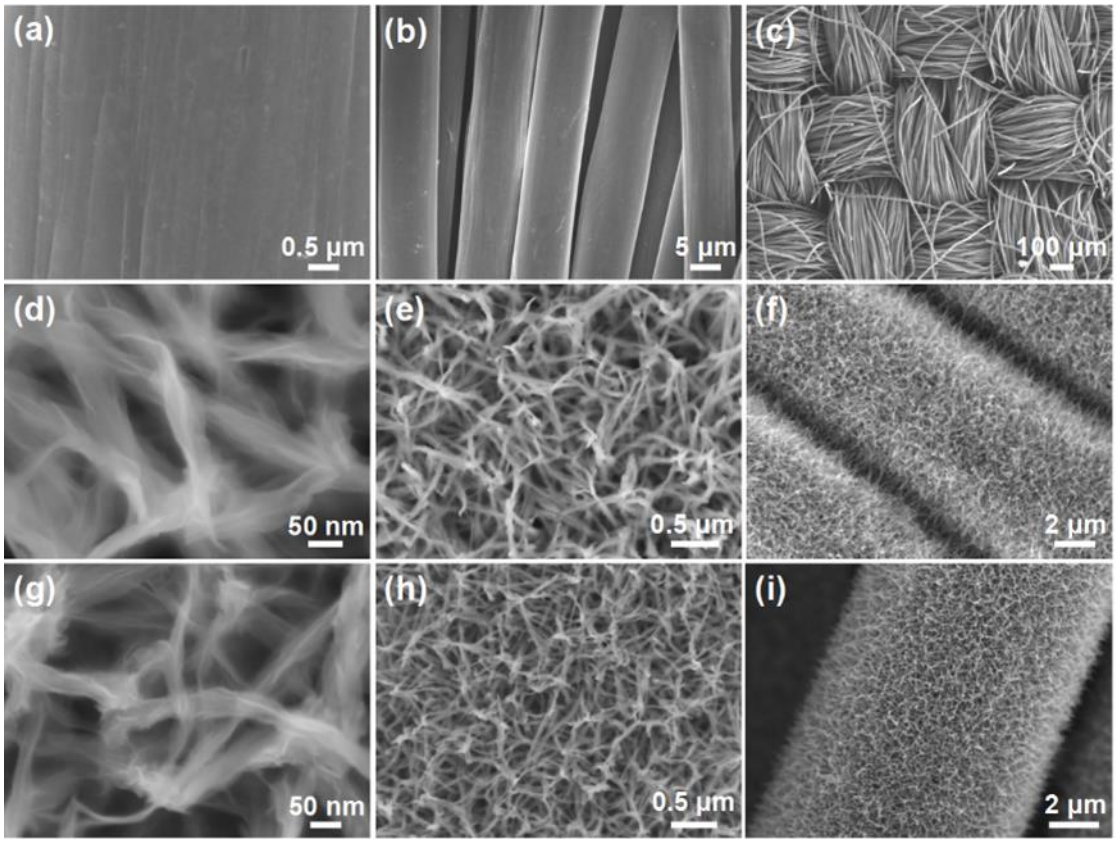

Figure S1. (a-c) SEM images of the pure carbon textiles; (b-f) SEM images of the $Na_2Ti_3O_7$ nanofiber arrays on carbon textiles; (g-i) SEM images of the $Na_2Ti_3O_7$@N-GQDs nanofiber arrays on carbon textiles.

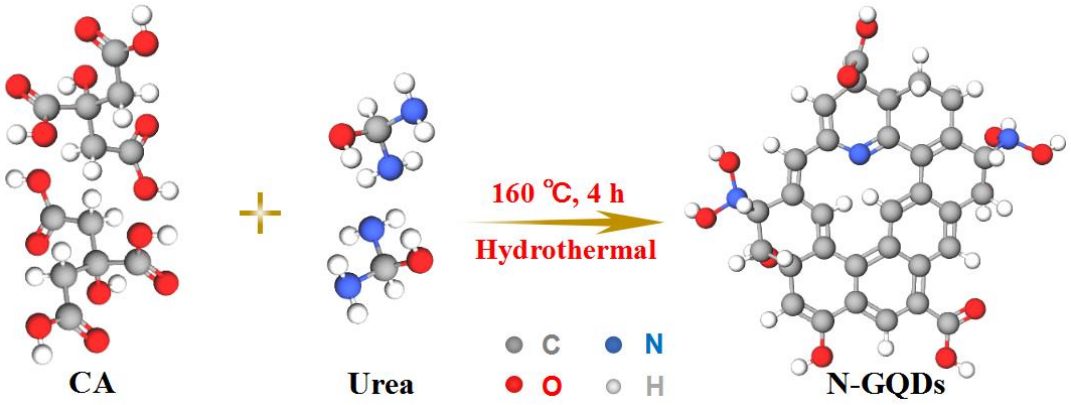

Figure S2. Illustration of the formation process of amine-functionalized N-GQDs via one-step pyrolysis of CA and urea.

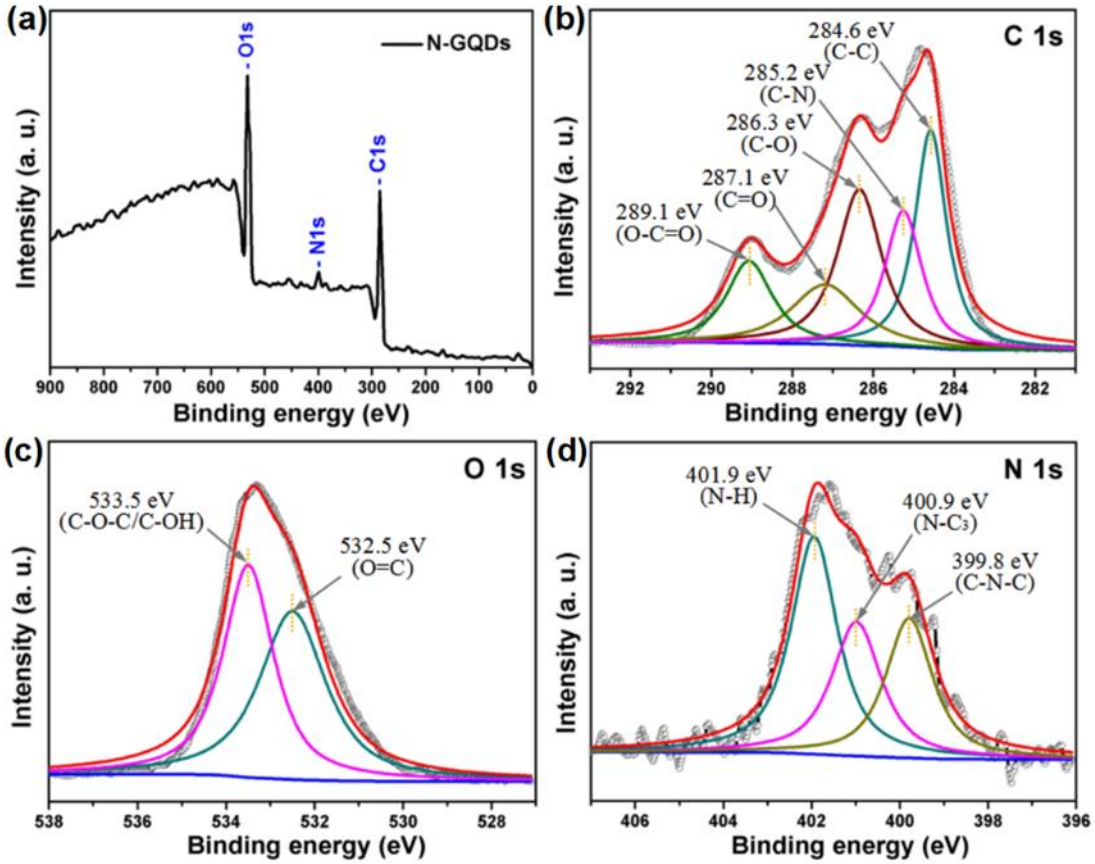

Figure S3. (a) Full-scan XPS spectrum of the N-GQDs; (b) C 1s XPS spectrum; (c) O 1s XPS spectrum; (d) N 1s XPS spectrum.

Figure S3a shows the survey spectrum of the N-GQDs, which have three typical peaks of C 1s at 284.6 eV, N 1s at 399.59 eV, and O 1s at 530.79 eV. The high-resolution C 1s spectrum of the N-GQDs (Figure S3b) revealed the presence of C-C (284.6 eV), C-N (285.2 eV), C-O (286.3 eV), C=O (287.1 eV) and O-C=O (289.1 eV) functional groups.[8] Moreover, the O 1s spectrum (Figure S3c) further confirmed these observations with two characteristic oxygen states of C=O (532.5 eV) and C-OH/C-O-C (533.5 eV).[8] The spectrum of N 1s (Figure S3d) in the N-GQDs indicated the presence of three relative nitrogen species of N-H (401.9 eV), N-C_3 (400.9 eV) and C-N-C (399.8 eV),[9] indicating the existence of amide groups and the doping of nitrogen atoms during the synthesis process.

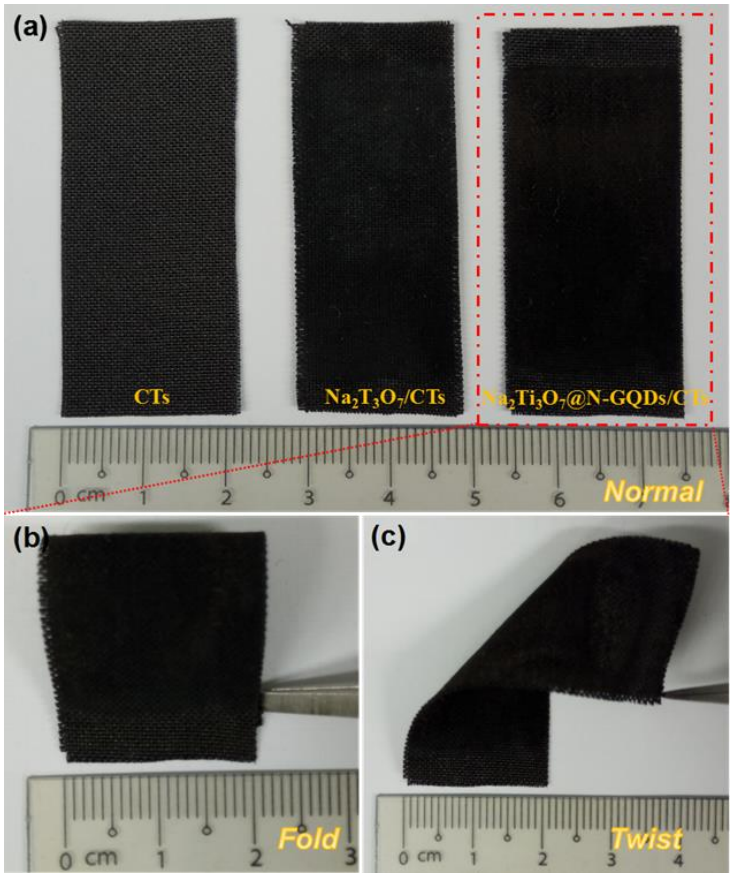

Figure S4. Optical images for the flexible electrode material. (a) Photographs of the formation processes of the $Na_2Ti_3O_7$@N-GQDs/CTs; (b,c) Digital photos: the electrode was folded and twisted.

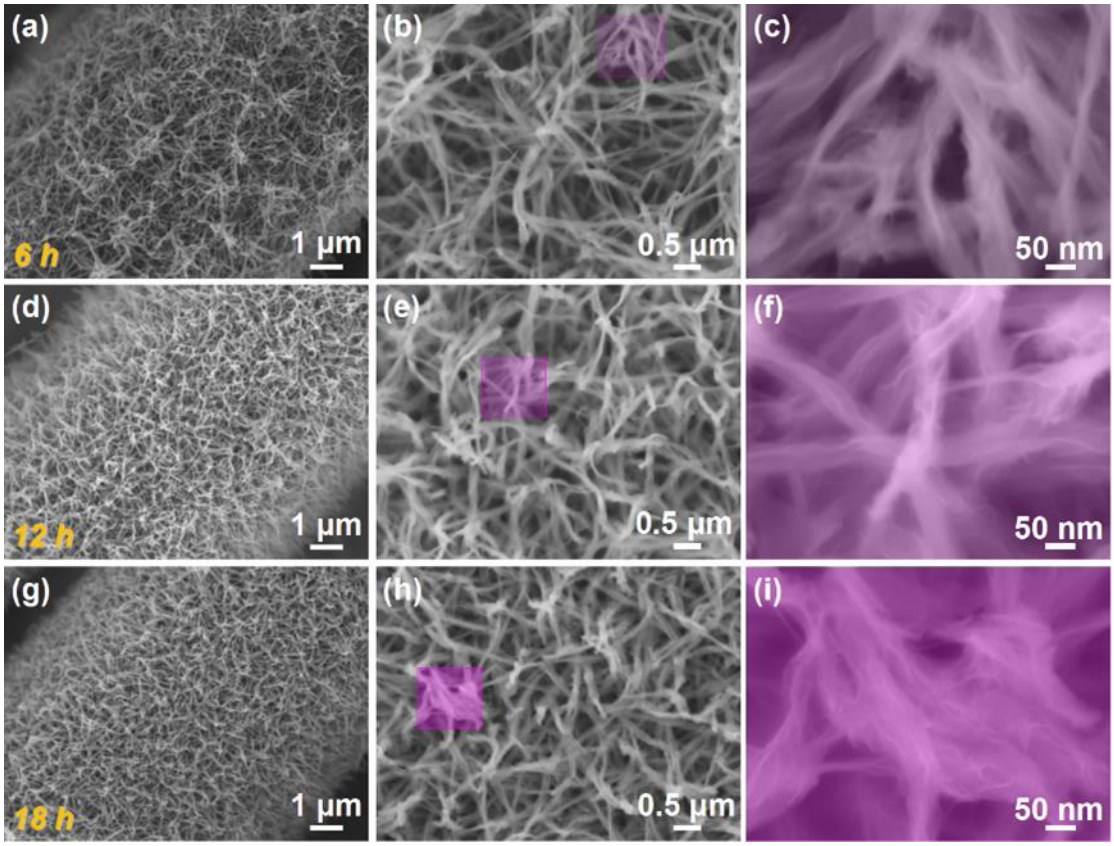

Figure S5. SEM images of the $Na_2Ti_3O_7$ nanofiber arrays on carbon textiles at various reaction stages by setting the reaction time to (a-c) 6 h, (d-f) 12 h, (g-i) 18 h.

The probable growth process of $Na_2Ti_3O_7$ nanofiber arrays on carbon textiles (CTs) has been investigated through a series of time-dependent experiments. Precursors were collected at different reaction time from 6 to 18 h, and then annealed under the same condition. The evolution of structure and morphologies were observed by SEM images in Figure S5. At the beginning of 6 h, many nanofiber arrays are grown on the surface of carbon textiles, but these nanofiber arrays grew sparsely and failed to completely cover the carbon textiles surface (Figure S5a-c). For the reaction time equal to 12 h, highly ordered $Na_2Ti_3O_7$ nanofiber arrays uniformly distributed on the CTs surface (Figure S5d-f). When the time extends to 18 h, filled with a great deal of nanofiber arrays crowded together, and the nanofibers gradually become wider and longer, as shown in Figure S5g-i. Thus, the morphology of $Na_2Ti_3O_7$ can be easily controlled through hydrothermal time.

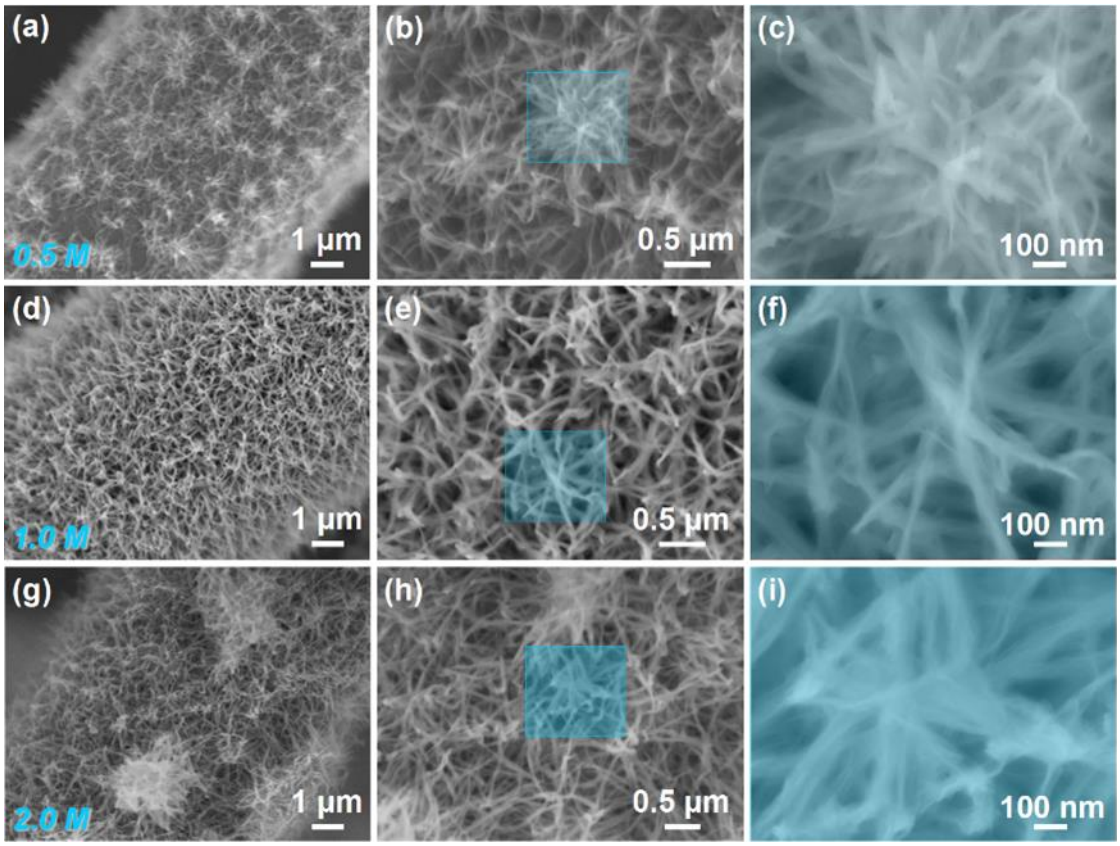

Figure S6. SEM images of the $Na_2Ti_3O_7$/CTs obtained with the same reaction stages except that different concentration ratios of aqueous mix solution (H_2O_2, NaOH and TBT) immersed in hydrothermal synthesis process: (a-c) 50 %, (d-f) 100 % and (g-i) 200 %.

To obtain the appropriate mass, uniform morphology, and well crystallinity $Na_2Ti_3O_7$/CTs electrodes, the reaction concentration have been optimized. Figure S6 shows the SEM images of $Na_2Ti_3O_7$/CTs reacted in 0.5, 1.0, and 2.0 M aqueous mix solution (H_2O_2, NaOH and TBT), respectively. Figure S6a-c displays numerous regular nanosize fibers grow on the surface of carbon textiles, but not completely cover. When the concentration of aqueous mix solution above 1.0 M, the carbon textiles surface is covered completely by $Na_2Ti_3O_7$ nanofiber arrays, as shown in Figure S6d-i. Significantly, the carbon textiles reacted in 1.0 M aqueous mix solution exhibit interconnected nanofibre arrays with uniform arrangement (Figure S6d-f). But some $Na_2Ti_3O_7$ nanoflowers can be derived from $Na_2Ti_3O_7$/CTs with appear in 2.0 M aqueous mix solution, implying excessive solvent addition.

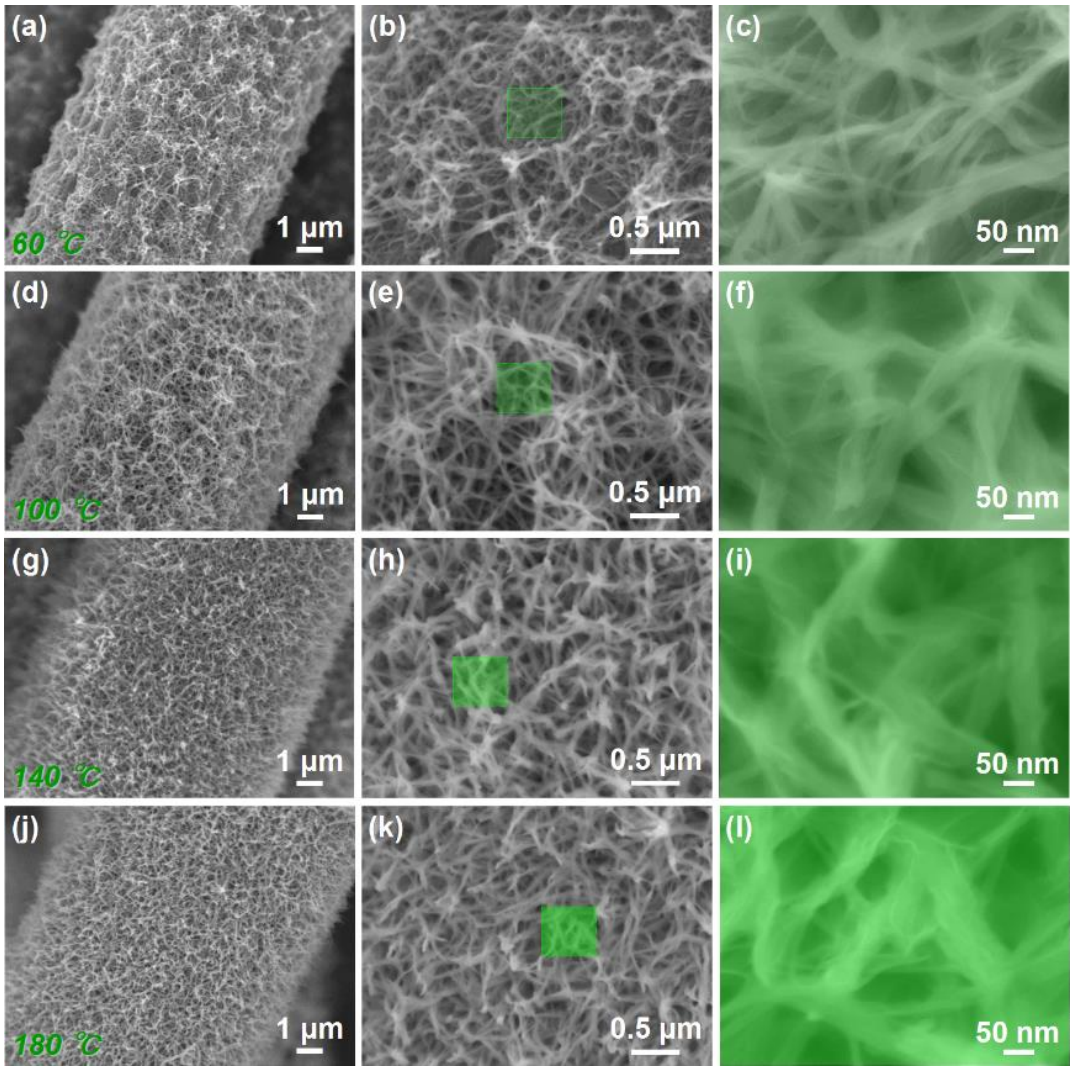

Figure S7. SEM images of the $Na_2Ti_3O_7$ nanofiber arrays on carbon textiles synthesized at various temperatures: (a-c) 60 °C, (d-f) 100 °C, (g-i) 140 °C and (j-l) 180 °C.

Figure S7 shows the SEM images of the $Na_2Ti_3O_7$ nanofiber arrays on carbon textiles synthesized at various temperatures. with the increasement of synthesized temperature, more $Na_2Ti_3O_7$ nanofiber arrays can be grow on carbon textiles. It is noteworthy that the obtained $Na_2Ti_3O_7$/CTs at 140 °C exhibits uniform morphology and appropriate load, but almost no change when the temperature was increased to 180 °C.

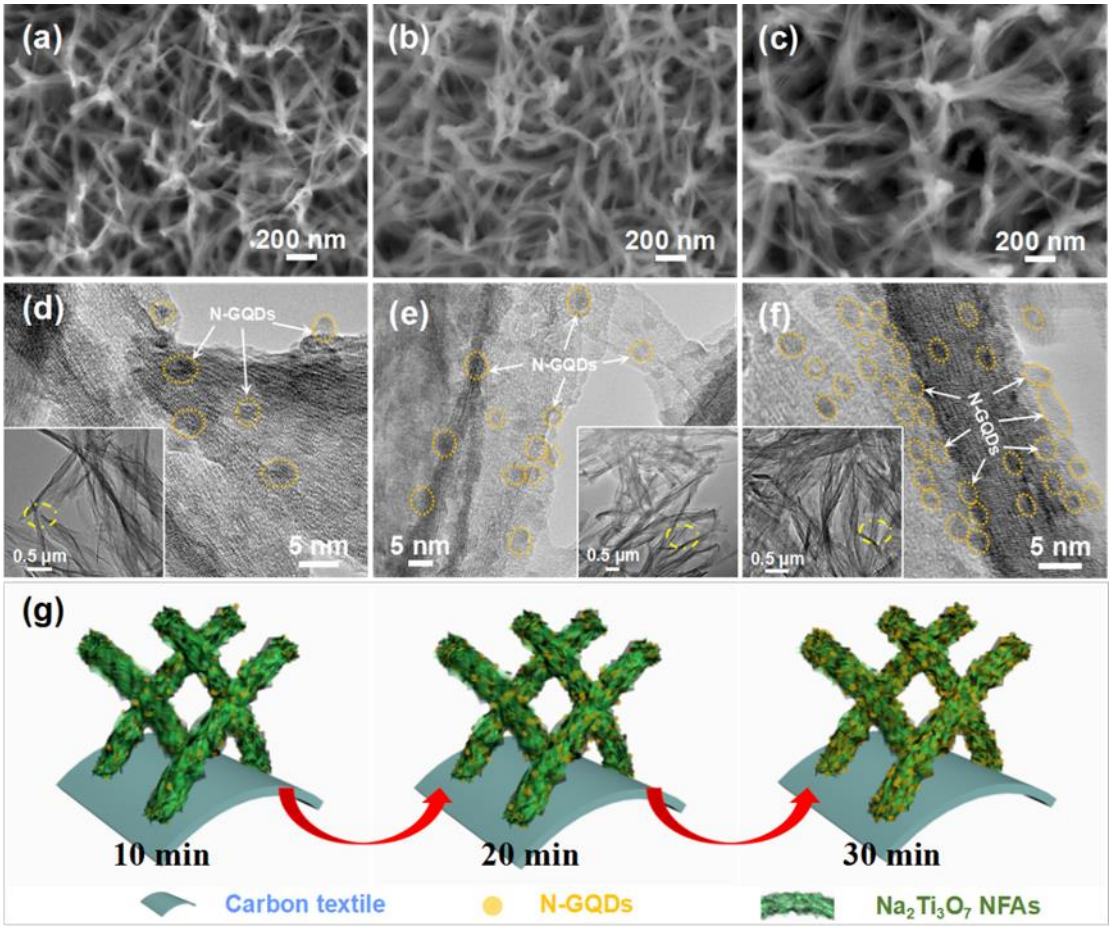

Figure S8. (a-c) SEM and (d-f) TEM images of the $Na_2Ti_3O_7$@N-GQDs/CTs synthesized at different electroplated time: 10 min, 20 min, and 30 min, respectively; (g) Proposed mechanism for the effect of deposited time on the morphology construction.

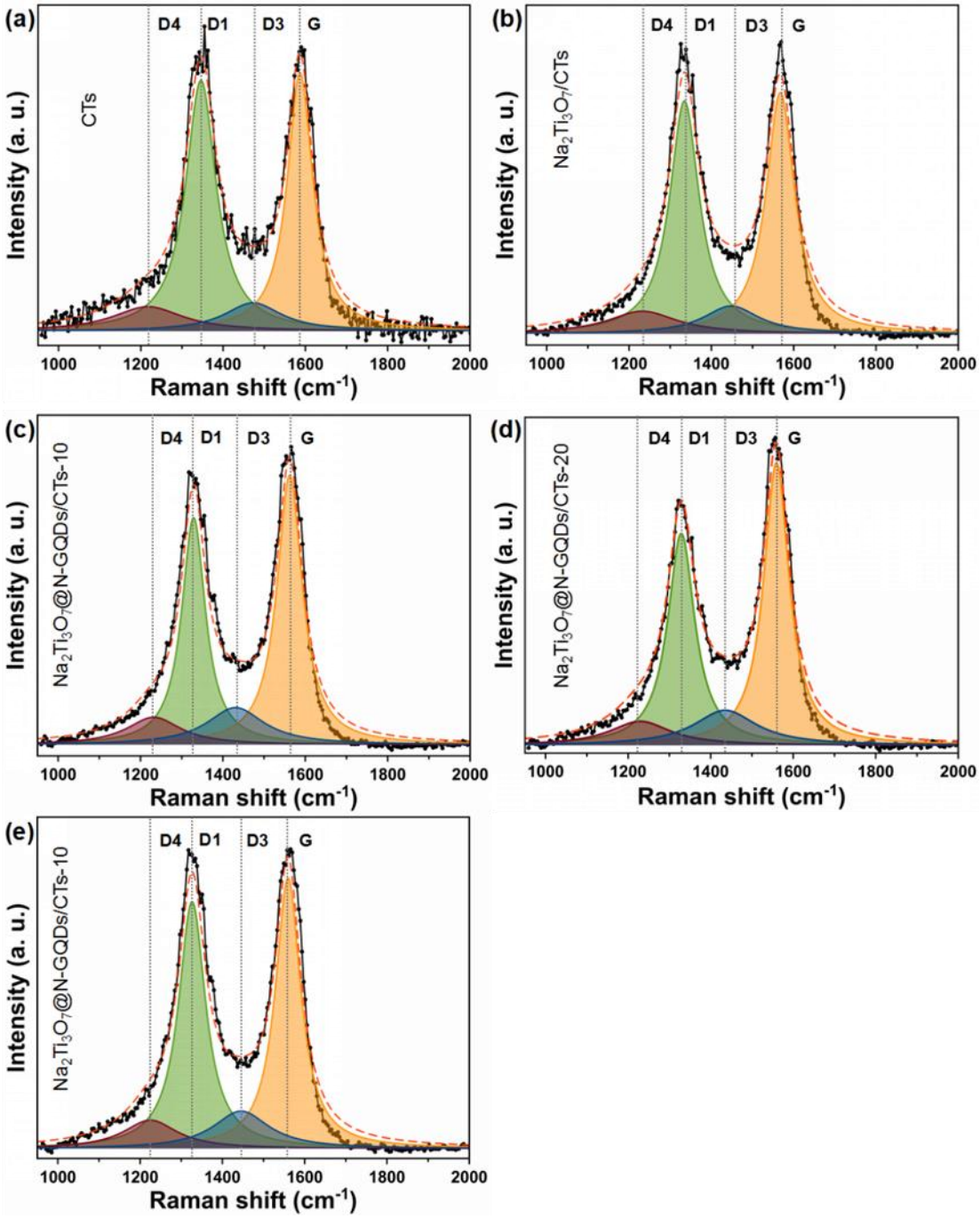

Figure S9. Curve fitting results of the Raman spectra of various samples: (a); CTs; (b) $Na_2Ti_3O_7$/CTs; (c) $Na_2Ti_3O_7$@N-GQDs/CTs-10; (d) $Na_2Ti_3O_7$@N-GQDs/CTs-30.

Specifically, the G band corresponds to the defect-free sp^2 carbon textiles with E_{2g} symmetry vibration mode. The D1 band with A_{1g} symmetry vibration mode is associated with the small crystallite sizes, grains, or edge plane defects of graphite domains.[10] The D3 band is assigned to amorphous carbon, while the presence of D4 band has been tentatively related to the existence of polyene-like structures or ionic impurities.[11] The intensity ratio of D1 and G band (I_{D1}/I_G) of various $Na_2Ti_3O_7$@N-GQDs/CTs samples decreases in the small range of 0.8-1.0 with the electrodeposition time, revealing a similar average domain size of graphite. At the same time we observed a moderate increase of the I_{D3}/I_G and I_{D4}/I_G ratios for sample $Na_2Ti_3O_7$@N-GQDs/CTs-10 and $Na_2Ti_3O_7$@N-GQDs/CTs-20 compared to samples obtained at longer electrodeposition time (Figure S9 and Figure S10), suggesting that these types of defects are more easily generated in this electrodeposition time. However, further increasing the electrodeposition time to 30 min leads to the decrease of these defects.

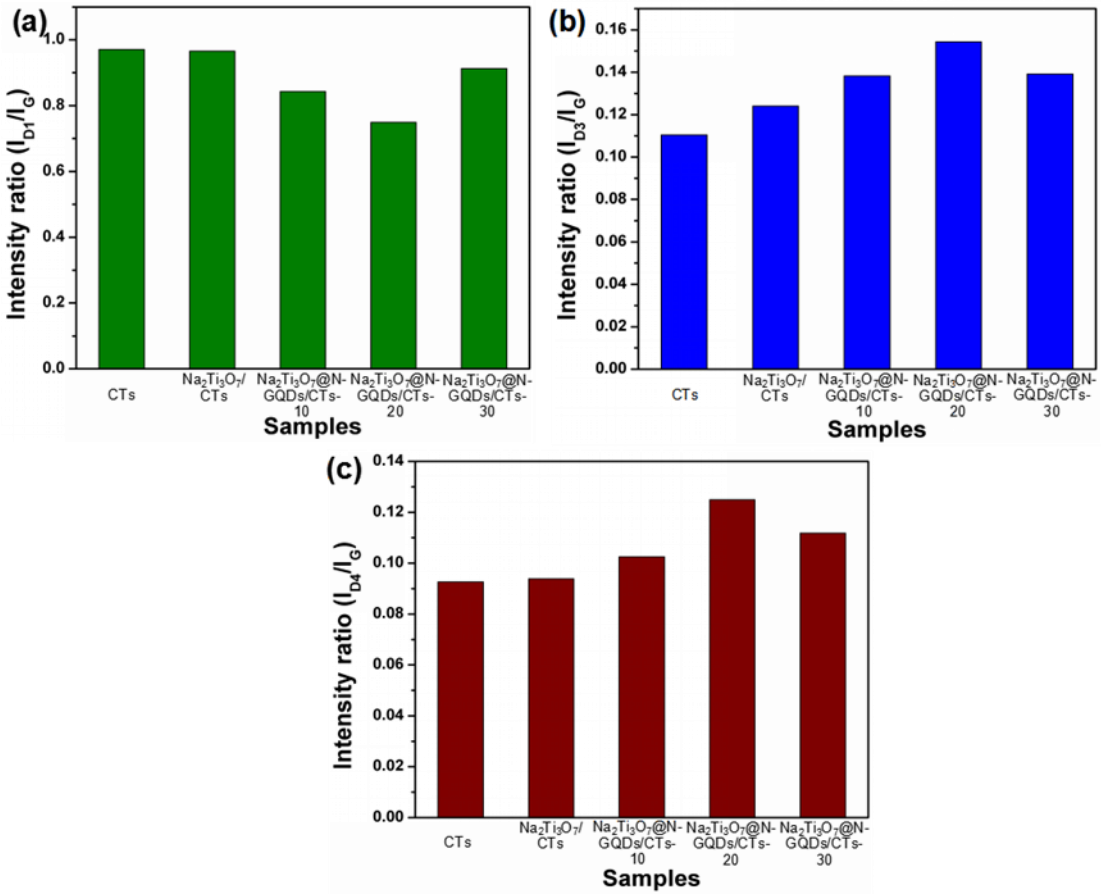

Figure S10. Intensity ratio of (a) I_{D1}/I_G, (b) I_{D3}/I_G and (c) I_{D4}/I_G.

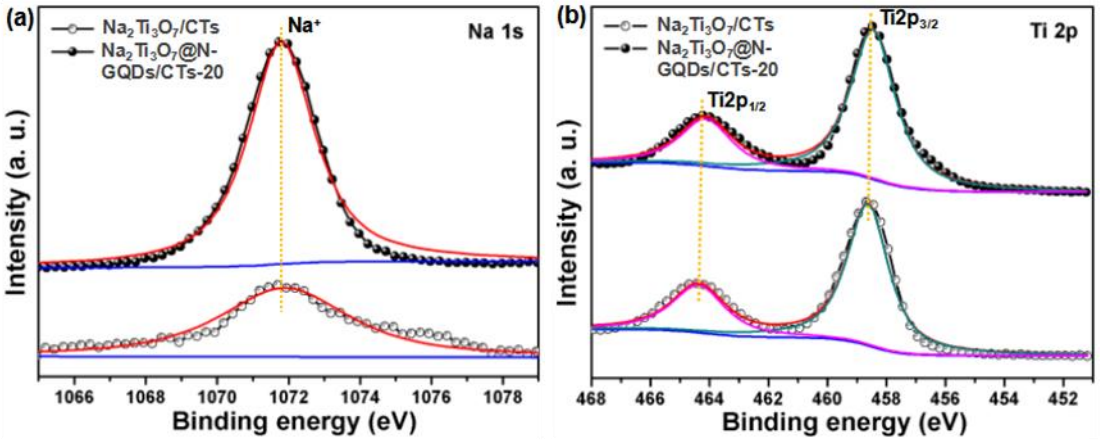

Figure S11. High-resolution XPS spectra of Na 1s (a) and Ti 2p (b) in the $Na_2Ti_3O_7$/CTs and $Na_2Ti_3O_7$@N-GQDs/CTs-20, respectively.

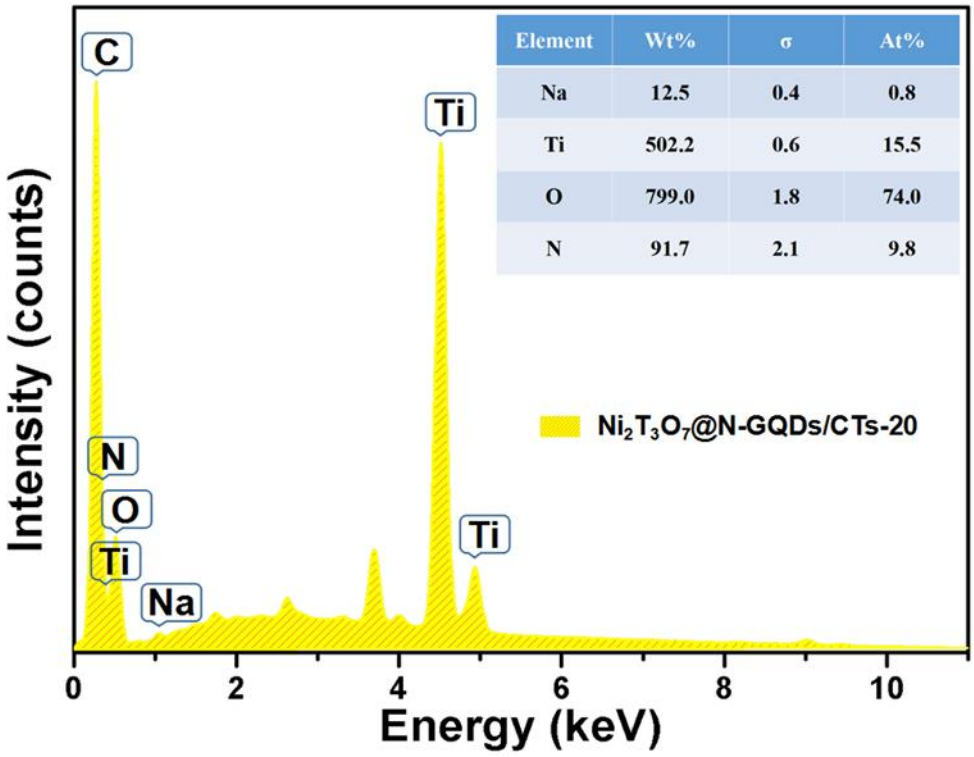

Element	Wt%	σ	At%
Na	12.5	0.4	0.8
Ti	502.2	0.6	15.5
O	799.0	1.8	74.0
N	91.7	2.1	9.8

Figure S12. EDS spectrum and the chemical composition of the 3D hybrid $Na_2Ti_3O_7$@N-GQDs/CTs-20 sample in Figure 3h.

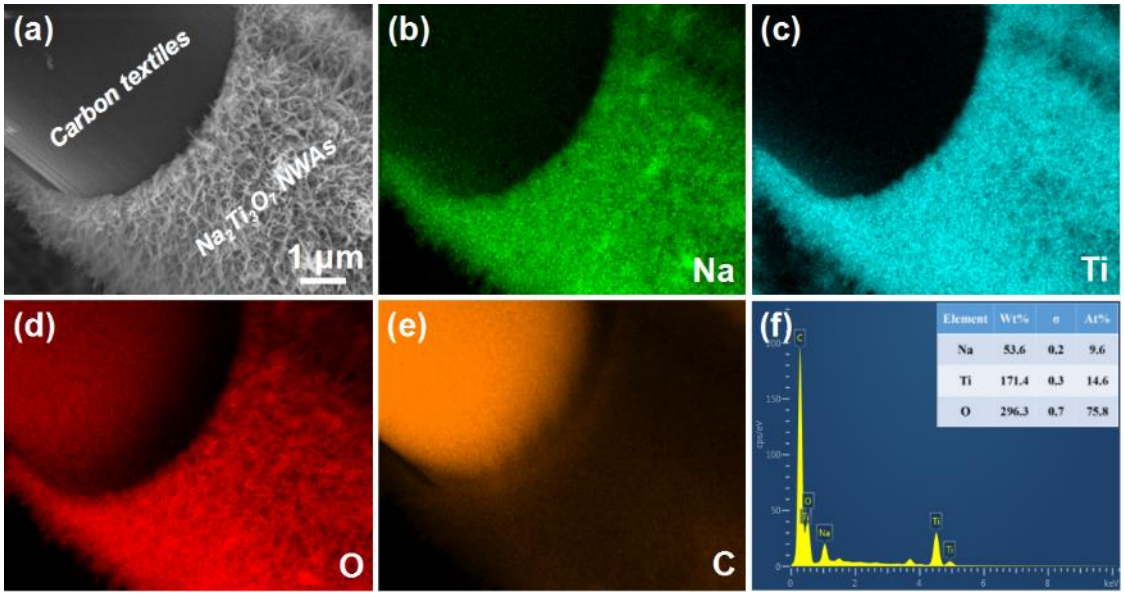

Figure S13. (a) Dark-field image of $Na_2Ti_3O_7$ NFAs on carbon textile; (b-e) EDS mapping of Na, Ti, O and C; (f) EDS spectrum and the chemical composition of the 3D hybrid $Na_2Ti_3O_7$/CTs sample.

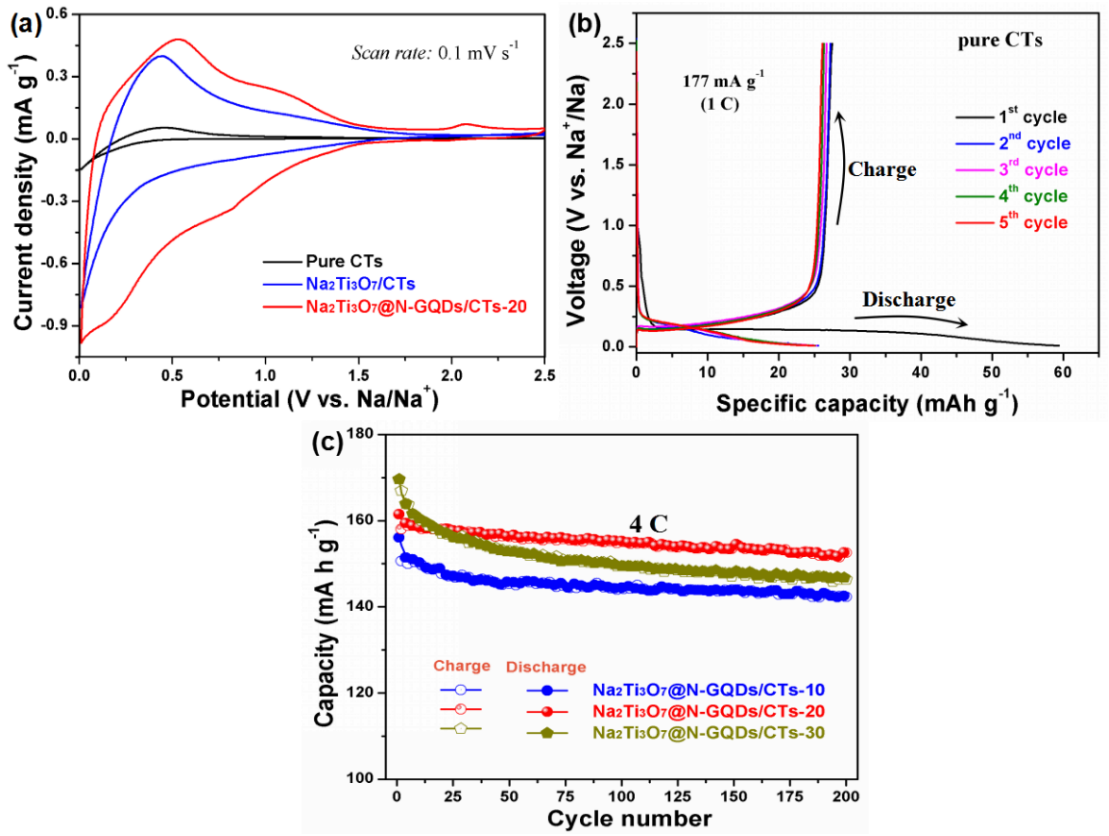

Figure S14. (a) The comparison of CV curves of three electrodes (including pure carbon textiles, $Na_2Ti_3O_7$/CTs and $Na_2Ti_3O_7$@N-GQDs/CTs-20) at the second cycle; (b) Galvanostatic charge/discharge profiles during the first five cycles of the pure CTs electrode; (c) Cycling performance of the $Na_2Ti_3O_7$@N-GQDs/CTs prepared in the different electroplated time (10 min, 20 min, and 30 min) electrodes at current density of 4 C.

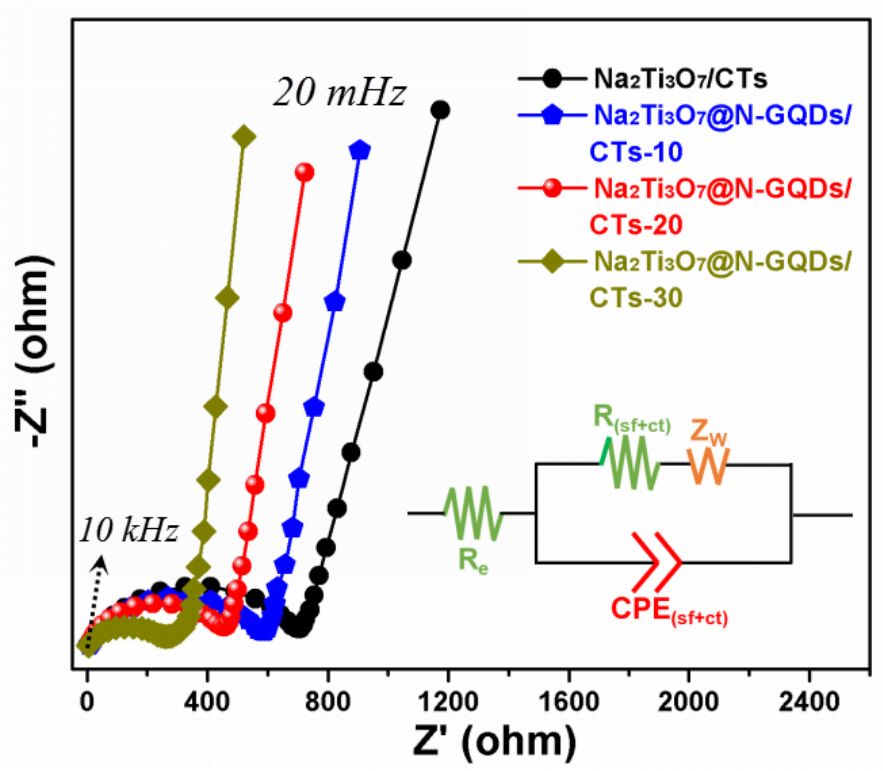

Figure S15. Nyquist plots and equivalent circuit (inset) after the first cycle used for the EIS analysis of the $Na_2Ti_3O_7$@N-GQDs/CTs, $Na_2Ti_3O_7$@N-GQDs/CTs-10, $Na_2Ti_3O_7$@N-GQDs/ CTs-20 and $Na_2Ti_3O_7$@N-GQDs/CTs-30 electrodes.

At full-charged state after the first cycle of $Na_2Ti_3O_7$@N-GQDs/CTs, $Na_2Ti_3O_7$@N-GQDs/CTs-10, $Na_2Ti_3O_7$@N-GQDs/CTs-20 and $Na_2Ti_3O_7$@N-GQDs/CTs-30 electrodes, as shown in Figure S15. The resistance is simulated using inset equivalent circuit of R_e, where R_e is the ohmic resistance of solution and electrodes, R_{sf+ct} is the charge transfer resistance, CEP_{sf+ct} is the double layer capacitance, and Z_W represents constant phase element.[13] Simulations indicate that the charge transfer resistance of $Na_2Ti_3O_7$@N-GQDs/CTs, $Na_2Ti_3O_7$@N-GQDs/CTs-10, $Na_2Ti_3O_7$@N-GQDs/CTs-20 and $Na_2Ti_3O_7$@N-GQDs/CTs-30

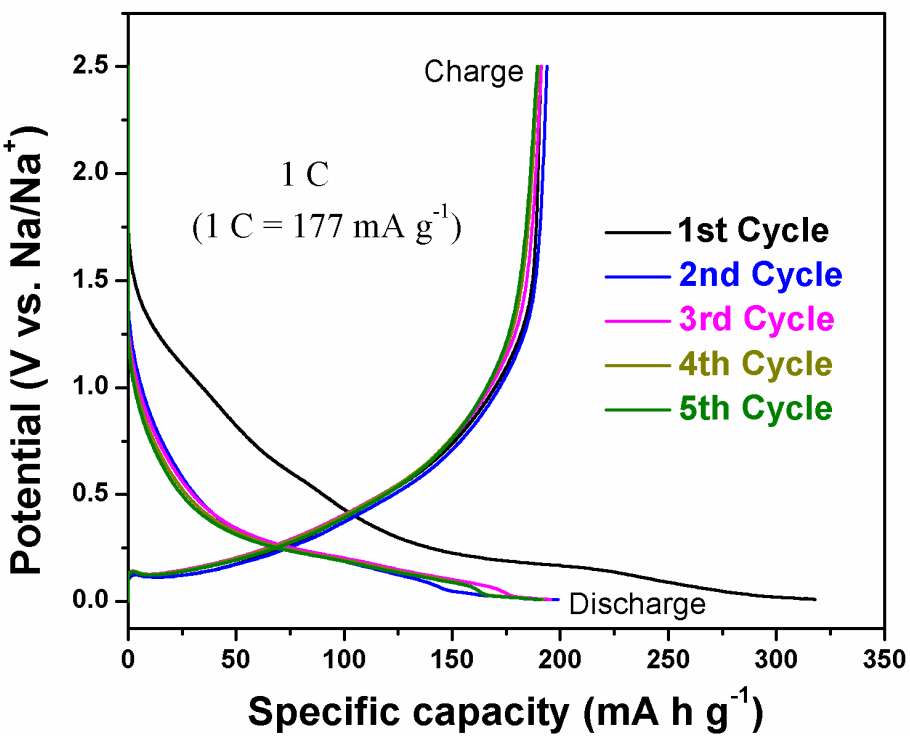

Figure S16. The first five discharge-charge profiles of the $Na_2Ti_3O_7$/CTs at a current density of 1 C.

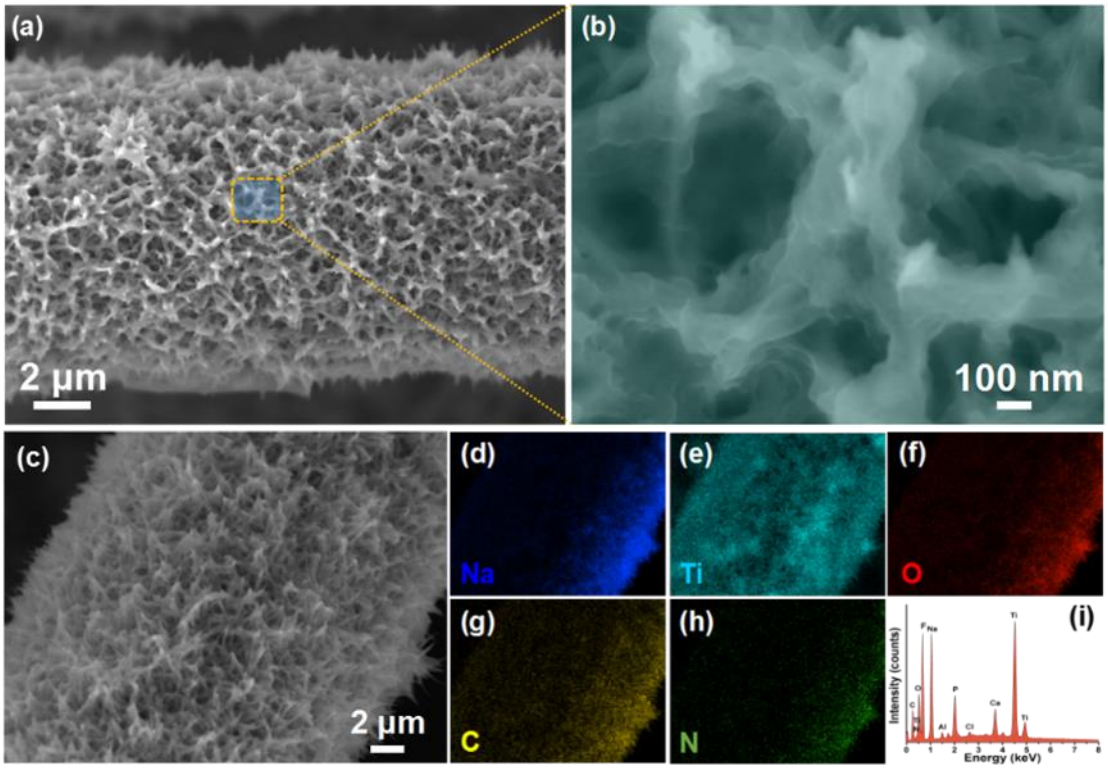

Figure S17. SEM image (a, b) and EDs mapping (c-i) of the $Na_2Ti_3O_7$@N-GQDs/CTs-20 electrode after 1000 cycles.

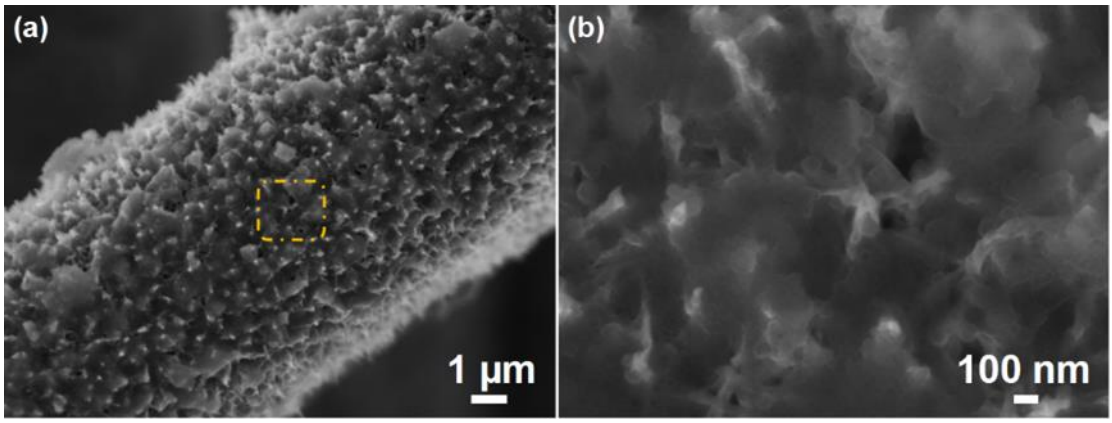

Figure S18. SEM images of the $Na_2Ti_3O_7$/CTs electrode after 1000 cycles.

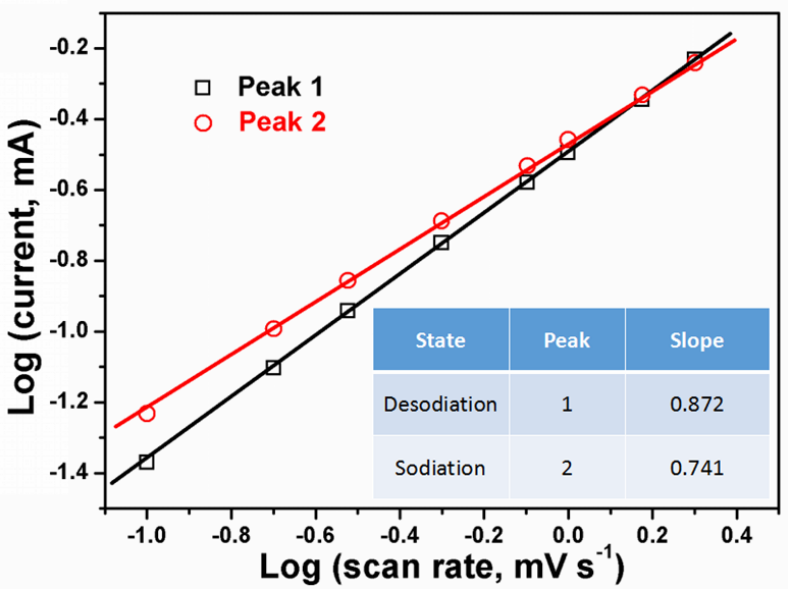

Figure S19. Log i vs. log v plots at different oxidation and reduction states of the $Na_2Ti_3O_7$@N-GQDs/CTs-20 electrode electrode.

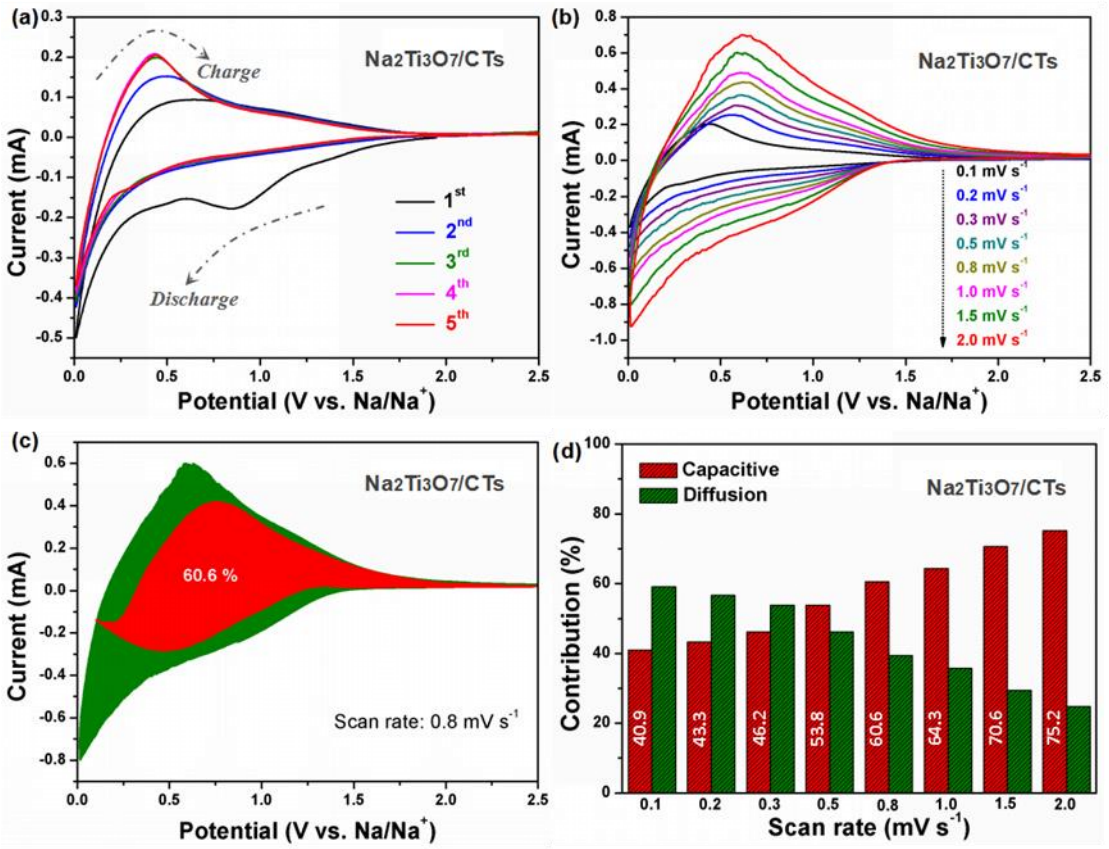

Figure S20. Electrochemical sodium-storage properties of $Na_2Ti_3O_7$/CTs electrode. (a) CV curves of the first five cycles of the $Na_2Ti_3O_7$/CTs electrode at a scan rate of 0.1 mVs^{-1}; (b) CV curves for Na^+ storage at different scan rate of the $Na_2Ti_3O_7$/CTs electrode; (c) Capacitive (red) and diffusion-controlled (green) contribution to charge storage of $Na_2Ti_3O_7$/CTs at 0.8 mV s^{-1}; (d) Normalized contribution ratio of capacitive (red) and diffusion- controlled (green) capacities of $Na_2Ti_3O_7$/CTs electrode at different scan rate.

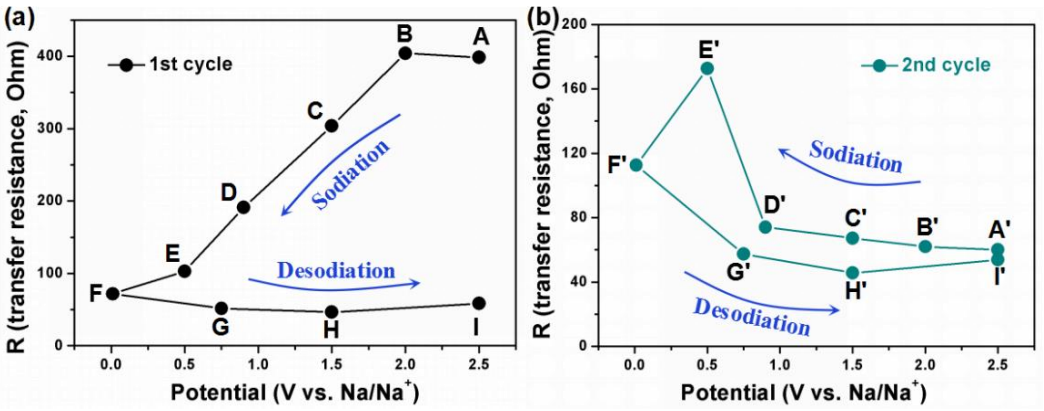

Figure S21. The corresponding change of charge transfer resistance at various points shown in Figure5 (c) and (d).

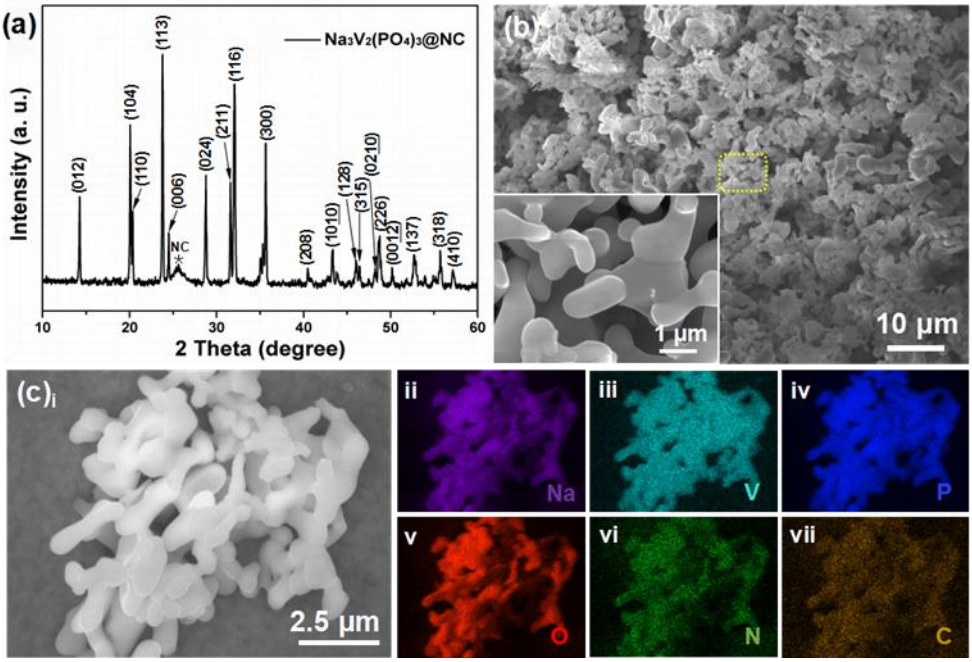

Figure S22. (a) XRD pattern and (b) SEM images of $Na_3V_2(PO4)_3$@NC powder; (c_i-c_{vii}) SEM image of $Na_3V_2(PO_4)_3$@NC powders and the corresponding EDS mapping of Na, V, P, O, N and C elements.

The XRD pattern of Na2V3(PO4)3@NC powder is shown in Figure S21a, which all show the diffraction peaks of Na3V2(PO4)3 (JCPDS card no. 01-070-3613).14 Moreover, a small and broad peak at 2θ ≈ 25.6 ° can be observed, which is attributed to the (002) planes of N-doped carbon (NC).15 The morphology of the Na2V3(PO4)3@NC powder was investigated with scanning electron microscopy, as shown in the inset Figure S21b. It can be seen that clusters-like Na2V3(PO4)3@NC is made up of many nanoparticles with particle size of 0.5-2 μm. The EDS mapping results in Figure S22ci-cvii clearly suggest that the elements Na, V, P, O, N and C are homogeneously distributed, confirming the Na2V3(PO4)3 core/NC shell hierarchical structure.

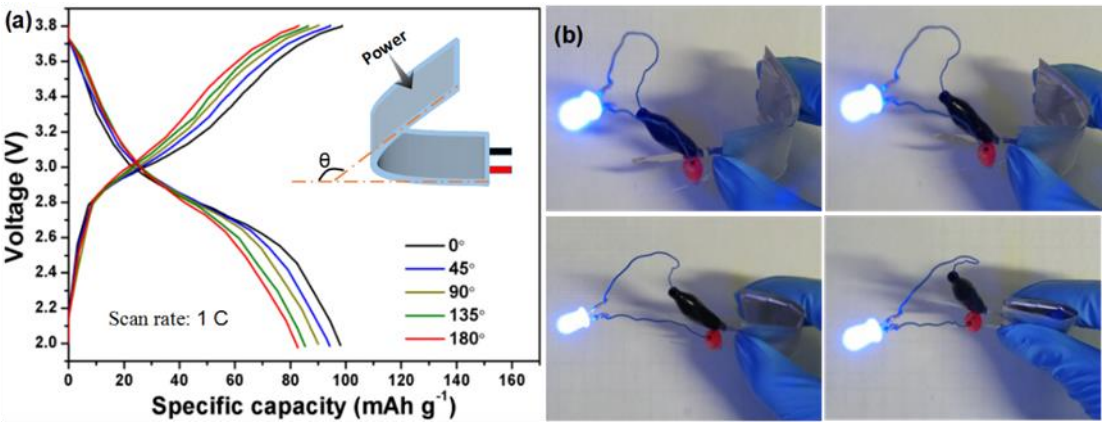

Figure S23. (a) The voltage versus specific capacity profiles of flexible full cell under different bending state: 0 °, 45 °, 90 °, 135 ° and 180 °; (b) The optical images show a light-emitting-diode (LED) lighting by a different bending state of the flexible full cell.

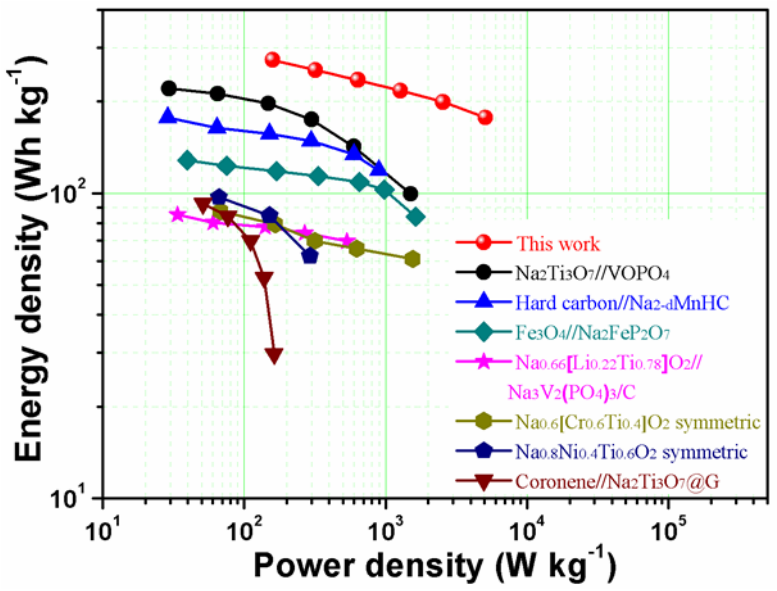

Figure S24. Energy density and power density of the $Na_2Ti_3O_7$@N-GQDs// $Na_3V_2(PO_4)_3$@NC full cell vs. other recently reported literatures.

Supporting Tables

Table S1 A survey of electrochemical properties of $Ni_2Ti_3O_7$ and its hybrid composites in sodium ion batteries. (1 C = 177 mA g^{-1})

Electrode description	Specific capacity (vs. Na/Na^+)	High-rate capacity (vs. Na/Na^+)	Cycling stability (%)	Ref.
$Ni_2Ti_3O_7$@N-GQDs/CTs-20	~342 mAh g^{-1} at 0.5 C between 0.01~2.5 V	~58 mAh g^{-1} at 64 C	92.5 % after 1000 cycles at 4 C	This work
Flower-like $Na_2Ti_3O_7$	~300 mAh g^{-1} at 0.1 A g^{-1} between 0.01~2.5 V	110 mAh g^{-1} at 3 A g^{-1}	69.5 % after 1000 cycles at 1 A g^{-1}	[12]
$Na_2Ti_3O_7$@C hollow spheres	210 mAh g^{-1} at 1 C between 0.01~2.5 V	63 mAh g^{-1} at 50 C	93.5 % after 1000 cycles at 50 C	[13]
Carbon-coated $Na_2Ti_3O_7$	219 mAh g^{-1} at 20 mA g^{-1} between 0.01~2.5 V	57 mAh g^{-1} at 2.0 A g^{-1}	~32.7 % after 200 cycles at 0.5 A g^{-1}	[14]
$Na_2Ti_3O_7$ nanotubes	220 mAh g^{-1} at 100 mA g^{-1} between 0.01~2.5 V	155 mAh g^{-1} at 2.0 A g^{-1}	~94.6 % after 100 cycles at 0.6 A g^{-1}	[15]
Hydrogenated $Na_2Ti_3O_7$ nanoarrays	225 mAh g^{-1} at 0.2 C between 0.01~2.5 V	71 mAh g^{-1} at 35 C	~91.5 % after 10000 cycles at 35 C	[16]
$Na_2Ti_3O_7$ nanowires@CNT	204.8 mAh g^{-1} at 0.2 C between 0.01~2.5 V	31.9 mAh g^{-1} at 10 C	~45.9 % after 10000 cycles at 2 C	[17]
$Na_2Ti_3O_7$@CNT coaxial nanocables	245 mAh g^{-1} at 170 mA g^{-1} between 0.01~2.5 V	100 mAh g^{-1} at 3.4 A g^{-1}	~66.7 % after 1000 cycles at 1.7 A g^{-1}	[18]
L-$Na_2Ti_3O_7$ NWs/CC	297.8 mAh g^{-1} at 0.5 C between 0.01~2.5 V	54.9 mAh g^{-1} at 5 C	~88.9 % after 300 cycles at 3 C	[19]

$Na_2Ti_3O_7$/rGO composite	325 mAh g^{-1} at 20 mA g^{-1} between 0.01~2.5 V	116 mAh g^{-1} at 2.0 A g^{-1}	~40.9 % after 300 cycles at 0.1 A g^{-1}	[20]
$Na_2Ti_3O_7$ nanoribbon array/graphene foam	~200 mAh g^{-1} at 200 mA g^{-1} between 0.01~2.5 V	~65 mAh g^{-1} at 4.0 A g^{-1}	~77.2 % after 2000 cycles at 2 A g^{-1}	[21]
$Na_2Ti_3O_7$	175 mAh g^{-1} at 0.1 C between 0.01~2.5 V	71 mAh g^{-1} at 5 C	~66.7 % after 50 cycles at 0.1 C	[22]

Supporting Reference

[1] Z. H. Li, W. Shen, C. Wang, Q. J. Xu, H. M. Liu, Y. G. Wang, Y. Y. Xia, J. Mater. Chem. A, 2016, 4, 17111-17120.

[2] Y. P. Zhang, L. Guo and S. H. Yang, *Chem. Commun.*, 2014, **50**, 14029-14032.

[3] J. Billaud, R. J. Clément, A. R. Armstrong, J. Canales-Vázquez, P. Rozier, C. P. Grey and P. G. Bruce, *J. Am. Chem. Soc.*, 2014, **136**, 17243-17248.

[4] F. Niu, J. Yang, N. N. Wang, D. P. Zhang, W. L. Fan, J. Yang and Y. T. Qian, *Adv. Funct. Mater.*, 2017, **27**, 1700522.

[5] T. Brezesinski, J. Wang, J. Polleux, B. Dunn and S. H. Tolbert, *J. Am. Chem. Soc.*, 2009, **131**, 1802-1809.

[6] H. S. Li, L. L. Peng, Y. Zhu, X. G. Zhang and G. H. Yu, *Nano Lett.*, 2016, **16**, 5938-5943.

[7] H. S. Li, L. L. Peng, Y. Zhu, D. H. Chen, X. G. Zhang and G. H. Yu, *Energy Environ. Sci.*, 2016, **9**, 3399-3405.

[8] L. P. Lin, M. C. Rong, S. S. Lu, X. H. Song, Y. X. Zhong, J. W. Yan, Y. R. Wang and X. Chen, *Nanoscale*, 2015, **7**, 1872-1878.

[9] L. B. Tang, R. B. Ji, X. M. Li, K. S. Teng, S. P. Lau, J. Mater. Chem. C, 2013, 1, 4908-4915.

[10] V. Perazzolo, C. Durante, R. Pilot, A. Paduano, J. Zheng, G. A. Rizzi, A.

Martucci, G. Granozzi, A. Gennaro, Carbon, 2015, 95, 949-963.

[11] Y. Xu, W. G. Tu, B. W. Zhang, S. M. Yin, Y. Z. Huang, M. Kraft, R. Xu, Adv. Mater., 2017, 29, 1605957.

[12] S. Y. Dong, L. F. Shen, H. S. Li, G. Pang, H. Dou, X. G. Zhang, Adv. Funct. Mater., 2016, 26, 3703-3710.

[13] F. X. Xie, L. Zhang, D. W. Su, M. Jaroniec, S. Qiao, Adv. Mater., 2017, 29, 1700989.

[14] C. S. Ding, T. Nohira, R. Hagiwara, J. Power Sources, 2017, 354, 10-15.

[15] H. S. Li, L. L. Peng, Y. Zhu, D. H. Chen, X. G. Zhang, G. H. Yu, Energy Environ. Sci., 2016, 9, 3399-3405.

[16] S. D. Fu, J. F. Ni, Y. Xu, Q. Zhang, L. Li, Nano Lett., 2016, 16, 4544- 4551.

[17] Z. H. Li, S. C. Ye, W. Wang, Q. J. Xu, H. M. Liu, Y. G. Wang, Y. Y. Xia, ACS Omega, 2017, 2, 5726-5736.

[18] S. Y. Dong, L. F. Shen, H. S. Li, P. Nie, Y. Y. Zhu, Q. Sheng, X. G. Zhang, J. Mater. Chem. A, 2015, 3, 21277-21238.

[19] Z. H. Li, W. Shen, C. Wang, Q. J. Xu, H. M. Liu, Y. G. Wang, Y. Y. Xia, J. Mater. Chem. A, 2016, 4, 17111-17120.

[20] Z. M. Zhou, H. M. Xiao, F. Zhang, X. L. Zhang, Y. B. Tang, Electrochim. Acta, 2016, 211, 430-436.

[21] S. Y. Dong, L. Y. Wu, J. J. Wang, P. Nie, H. Dou, X. G. Zhang, J. Mater. Chem. A, 2017, 5, 5806-5812.

[22] A. Rudola, K. Saravanan, C. W. Mason, P. Balaya, J. Mater. Chem. A, 2013, 1, 2653-2662.